Supplemental Information
Supplemental Experimental Procedures

Reagents Lipid Administration and Flow Cytometry (Yeast cells) – continued.
Analytical flow cytometry was performed using a three-laser BD LSRII (BD Biosciences) operating on the FACS Diva 6.1.3 software package. Forward and side-scatter were used to identify single cell populations as illustrated in (fig S12): note, different settings were required to isolate *S.cerevisiae* and *S.pombe* single cells. Experiments were gated with both cell controls and single cell populations selected during data analysis. PI was used to exclude dead cells from analysis, and NBD-lipid uptake was measured using a FITC filter set (530/30 nm band-pass filter with 525 nm long-pass filter). At least 10,000 cells were analyzed per experimental replicate.

Inhibitor experiments were performed essentially as outlined above, except the NBD-lipid media was not pre-chilled prior to cellular administration to ensure solubility of the inhibitors during cell application. Lipid inhibitors were solubilized in 100% ethanol and added to SD supplemented with NBD-lipid probes at the indicated final concentrations. The final concentration of ethanol in all assay mixtures was 2.2%. The lysoSM and GlcSph inhibitors were selected because their critical micelle concentrations were determined to be compatible with the lipid uptake assay.

NBD-GlcCer colocalization microscopy.
Cells were cultured and administered NBD-lipids as outlined above. Once NBD-lipid incubation was completed, the cells were washed three times in 4% BSA-SA and twice with SA. The final cell pellets were resuspended in 10 µl of SA and maintained on ice for imaging before being mounted on glass slides and being imaged at room temperature. Images were acquired using a DeltaVision Elite system (GE Healthcare) using an Olympus 100x/1.4 NA UPLS Apo objective using FITC and A594 dichroic filters and deconvolved using SoftWoRx software (GE Healthcare). Post-acquisition analyses and presentation were prepared using Image J (NIH) in accordance to published ethical guidelines (1).

Surface biotinylation.
Cell surface biotinylation assays were performed as described previously (2). Cells were washed three times with chilled PBS containing 0.1 mM $CaCl_2$ and 0.1 mM $MgCl_2$ (PBS++) and incubated with 2 mM sulfo-NHS-LC-biotin (Thermo Scientific) in PBS++ at 4°C for 30 min - 2 h. To stop the biotinylation, the cells were washed three times with chilled PBS++ containing 100 mM glycine and 0.3% BSA, and then washed twice more with chilled PBS. The cells were then lysed in lysis buffer (20 mM HEPES-KOH [pH 7.4] containing 1% NP-40, 150 mM NaCl, and protease inhibitor cocktail [Nacalai Tesque]) for 30 min at 4°C. The lysates were centrifuged at maximum speed at 4°C for 20 min in a microcentrifuge to remove cellular debris and insoluble materials. Protein concentration of lysates were determined by BCA protein assay (Nacalai Tesque) and 400 µg of proteins were used. To precipitate the biotinylated proteins, the supernatant was incubated at 4°C for 2 h with streptavidin-agarose beads (Thermo Scientific) pre-equilibrated with lysis buffer. The streptavidin beads were washed three times with lysis buffer, once with high-salt buffer (20 mM HEPES-KOH [pH 7.4], 500 mM NaCl, 1 mM EDTA, 0.5% NP-40), and once with 20 mM HEPES-KOH, pH 7.4. Proteins were eluted from the beads with SDS-PAGE sample buffer, denatured at 25°C for 16 h, and subjected to immunoblot analysis.

Sequence Alignments and Phylogeny Analysis.
Protein sequences were collected from National Center for Biotechnology Information (NCBI) or UniProt, alignments performed using the ClustalW method (www.genome.jp/tools/clustalw/), and phylogenic analyses were performed using the tools provided on the same website. NCBI or Uniprot reference sequence accession numbers for each member of the alignment and phylogeny tree are as follows: Sp Dnf1 (Q9UT43.2), Sp Dnf2 (Q09891.1), Sp Dnf2.5 (NP_594759.1), Sp Drs2 (NP_596486.1), Sp Neo1 (Q10309.1); Sc Dnf1 (NP_011093.3), Sc Dnf2 (NP_010378.1), Sc Dnf3 (NP_013885.1), Sc

Drs2 (NP_009376.2), Sc Neo1 (P40527); Hs ATP8A1 (Q9Y2Q0), Hs ATP8A2 (Q9NTI2.2), Hs ATP8B1 (O43520), Hs ATP8B2 (P98198), Hs ATP8B3 (Q6UQ17), Hs ATP8B4 (NP_079113.2), Hs ATP9A (O75110), Hs ATP9B (O43861), Hs ATP10A (NP_077816.1), Hs ATP10B (NP_079429.2), Hs ATP10D (Q9P241), Hs ATP11A (P98196.3), Hs ATP11B (NP_055431.1), Hs ATP11C (Q8NB49). Logo alignments were generated with http://weblogo.berkeley.edu/logo.cgi (3) using a master alignment of P4-ATPases.

Lipid Extraction and thin layer chromatography.
NBD-PLs were administered as outlined above for yeast flow cytometry applications and washed twice with 4% BSA-SD, then resuspended in SD and placed on ice, as indicated. Following the washes, chase timepoints were taken by extracting lipids using a modified Bligh and Dyer method. Following resuspension in SD, 0.5 ml cell suspension cultures were mixed with 2 ml of methanol:chloroform (2:1) at the indicated timepoints. The mixtures were shaken at 30°C for 10 min to facilitate extraction, vortexed vigorously, and centrifuged for 5 min at 1,000 rpm to pellet cellular debris. The supernatant was removed and mixed with 0.5 ml chloroform and 1.5 ml 0.9% NaCl (wt/vol). After vortexing to mix, the mixture was centrifuged for 5 min at 1,000 rpm and the aqueous phase removed. The organic phase was evaporated in a Savant speed vac centrifuge, resuspended in 10 µl of methanol:chloroform (2:1). 5 µl of each sample and ~0.025 µg of the designated standard were spotted onto the TLC plates. Separations were performed using a chloroform:methanol:ammonium hydroxide mobile phase (65:25:4), dried, and visualized using a BioRad Gel Doc EZ Imager running software Image Lab version 5.2.1. Plates were digitally imaged below saturation using the manufacturer's SYBR Green. TLC digital images were exported as .tif files and spot quantification was performed using densitometry analysis using ImageJ (National Institutes of Health). Background density was taken from an area of the plate without sample, and subtracted from each spot reading. Trios of plates performed in parallel were imaged under the same settings, and the data were normalized to 0 min timepoint of the vector control NBD-GlcCer spot to compare between experiments and exposures. Total lane signal was taken by measuring density from each lane, starting from the spot up to the solvent front (indicated in Fig. S3B). Signal intensity from the 0min timepoint for each experiment was set at 1.0, and all other measurements were normalized to this value and assessed. All data analyses and statistical assessments were performed using a combination of GraphPad Prism 6 and Microsoft Excel.

Data availability. The primary data will be available upon request. Homology models will be available for download from the Graham lab (https://my.vanderbilt.edu/grahamlab/) and Shin lab (http://www.pharm.kyoto-u.ac.jp/hshin/ShinIndex.html) websites. The substrate transport measurements for all *S. cerevisiae* Dnf1 and Dnf2 enzyme variants are included in supplementary Tables 3 and 4, and the *S. cerevisiae* Dnf1 homology model was published previously and is available for download on a publicly accessible server. No material transfer agreements are required for data accessibility.

Data Analysis
All statistical analyses were performed using GraphPad Prism 6. A one-way ANOVA was run to assess variance in all data sets, and Tukey's post hoc analysis used for comparisons. Linear regression fits were used to assess rates of substrate uptake in Figure S7.

Supplemental Data

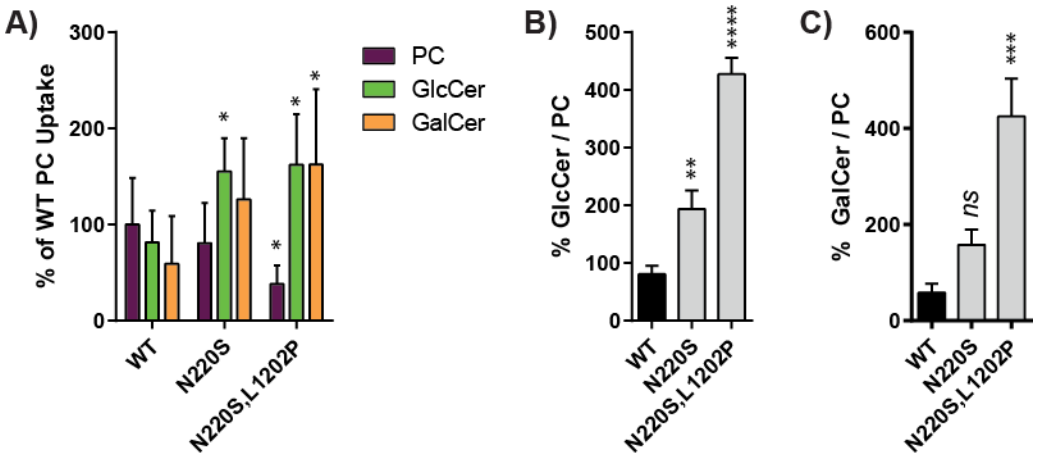

Figure S1. Sphingosine backbone gain-of-function mutations in Dnf1 enhance existing selection and preference for NBD-glycosphingolipids. pRS313-DNF1^{+} was expressed in a *dnf1,2Δ* background and its transport of NBD-PC, NBD-GlcCer, and NBD-GalCer was normalized to vector controls. (**A**) Dnf1 WT was compared to two Dnf1 mutant variants that were previously established to discriminate the sphingosine backbone. Ratiometric analyses of NBD-glycosphingolipid transport relative to NBD-PC revealed that the gain-of-function substitutions enhanced the preference for NBD-GlcCer (**B**) and NBD-GalCer (**C**). n≥6 ± SD. A one-way ANOVA was performed to assess variance and comparisons to WT were made with Tukey's post hoc analysis. * indicates $p < 0.05$, ** $p<0.01$, *** $p < 0.001$, and **** $p < 0.0001$.

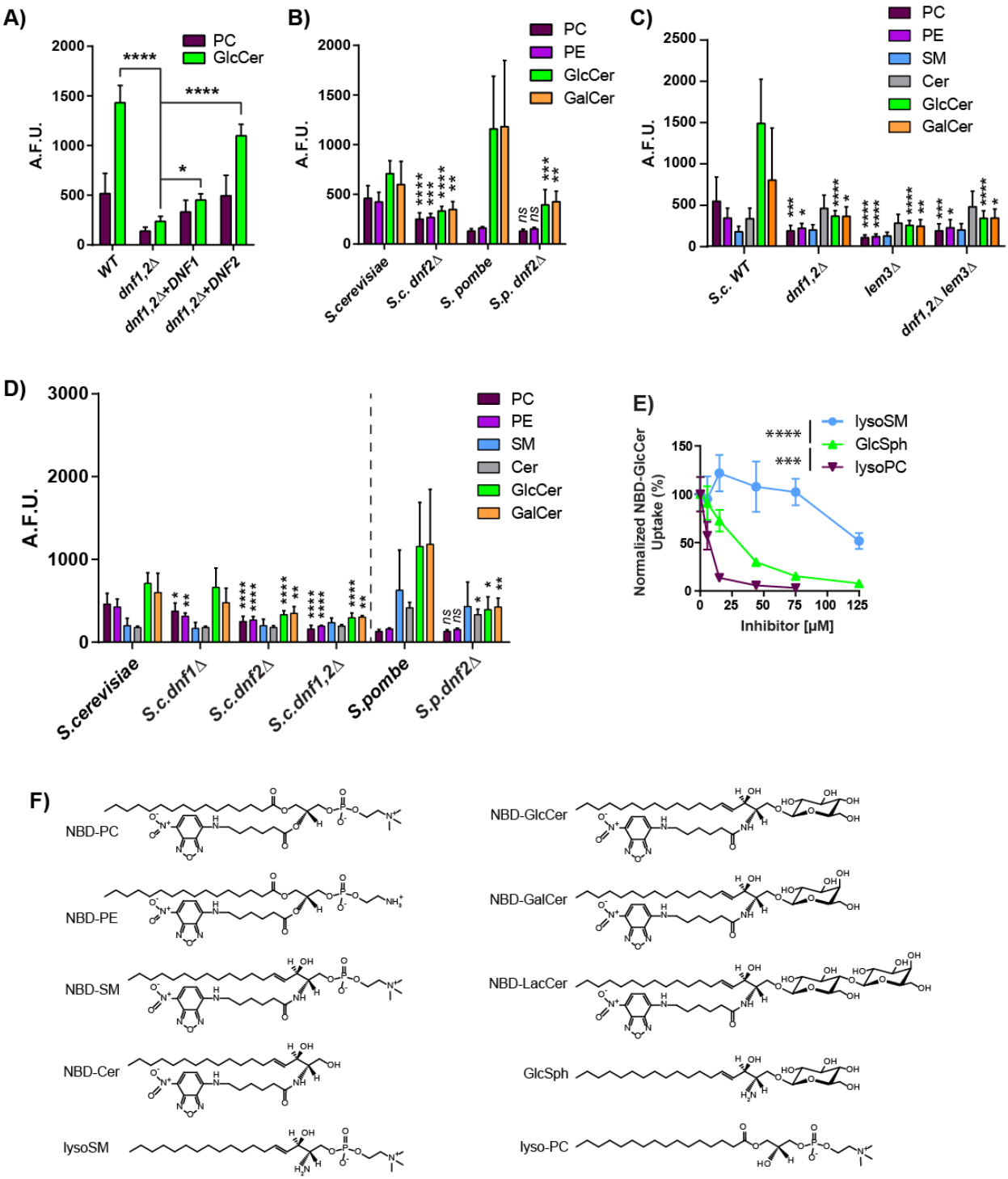

Figure S2. P4-ATPase KO in *S. cerevisiae* and *S. pombe* reveal conserved glycosphingolipid transport. (**A**) Plasmid-borne expression of DNF1 and DNF2 complements cellular uptake of NBD-PC and NBD-GlcCer in *dnf1,2Δ* background, n=6 ± SD, (arbitrary fluorescent units: A.F.U.). (**B**) Raw NBD-lipid uptake analyses of *S. cerevisiae* and *S. pombe WT* and *dnf2Δ* strains, n≥9 ± SD. *S. cerevisiae dnf1Δ* and *dnf2Δ* strains exhibit decreases in both PC and PE glycerophospholipids as well as GlcCer and GalCer glycosphingolipids (*dnf2Δ*). (**C**) Mutations in the dnf1,2 beta subunit, *lem3*, reduce NBD-PC, NBD-PE, NBD-GlcCer, and NBD-GalCer transport, n=6 ± SD. (**D**) Conversely, *S. pombe dnf2Δ* did not

alter glycerophospholipid transport, yet significantly decreases glycosphingolipid transport, n≥9 ± SD. (**E**) NBD-GlcCer uptake was tested in *S.c. dnf1,2Δ* cells expressing empty vector or DNF2, and transport was inhibited with increasing concentrations of lysoPC and GlcSph, but not lysoSM, n≥6 ± SD. (**F**) The chemical structures of all lipids analyzed in this study are presented. Avanti catalog numbers: NBD-PC (#810130), NBD-PE (#810153), NBD-SM (#810218), NBD-Cer (#810209), NBD-GlcCer (#810222), NBD-GalCer (#810220), NBD-LacCer (#810226), lysoSM (#860600), GlcSph (#860535), lysoPC (#855675). A one-way ANOVA was performed to assess variance and comparisons to WT were made with Tukey's post hoc analysis (B,C,D). Pairwise comparisons between WT and KO *S. cerevisiae* and *S. pombe* strains were made with an unpaired Student's t test (B). Inhibition data sets in (E) were assessed using a Two-way ANOVA with a Tukey's comparison. * indicates $p < 0.05$, ** $p<0.01$, *** $p < 0.001$, and **** $p < 0.0001$. *ns* highlights no significance.

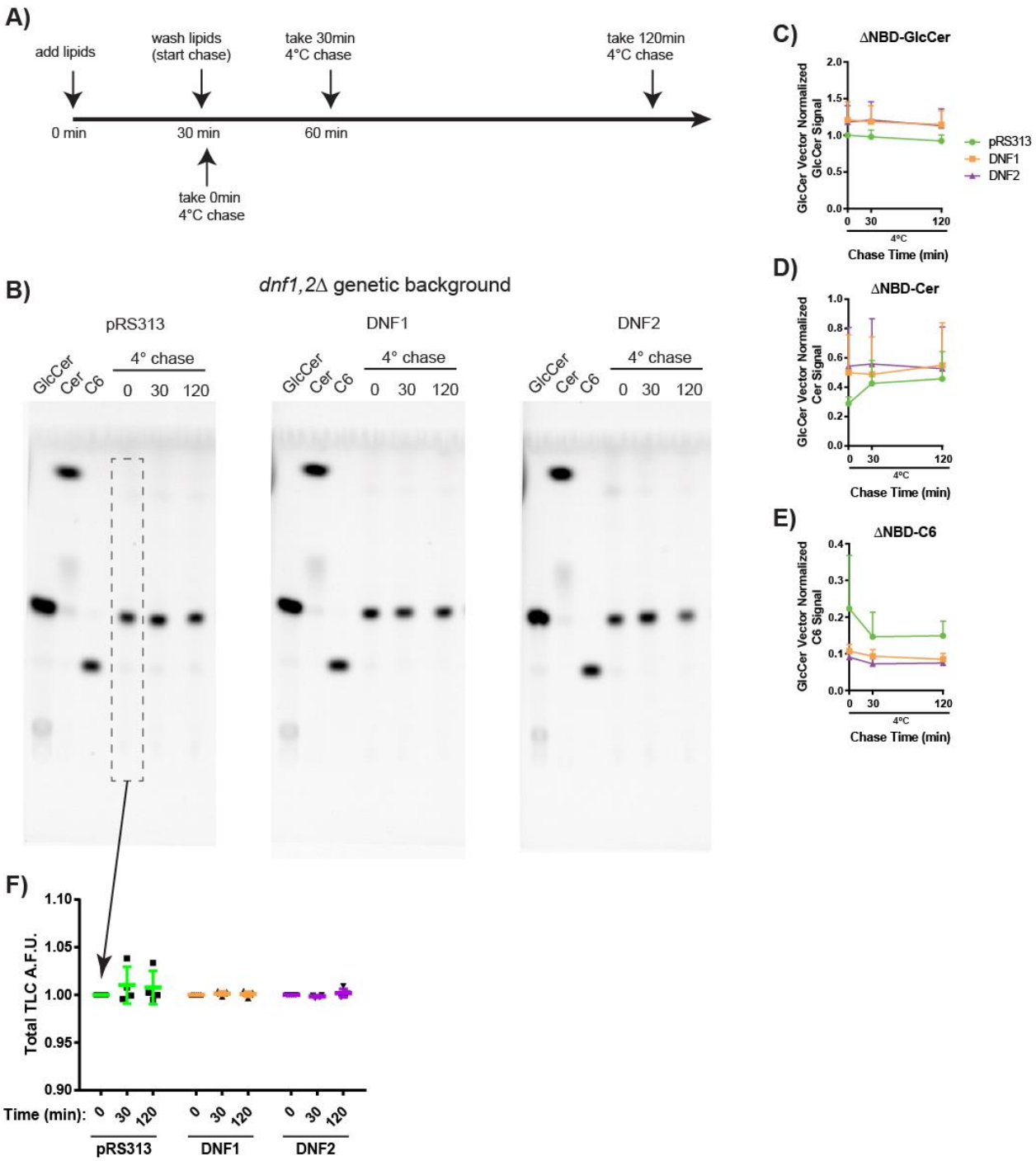

Figure S3. NBD-GlcCer is not appreciably metabolized over 120 min following administration. *dnf1,2Δ* cells expressing pRS313 vector, pRS313-DNF1, or pRS313-DNF2 were pulsed with NBD-GlcCer for 30 min on ice, washed, and incubated on ice. (**A**) Cells on ice were harvested at 0 min, 30 min, and 120 min for lipid extraction. (**B**) Extracts were separated by thin layer chromatography (TLC) and visualized, revealing very little metabolism of the NBD-GlcCer substrate, with quantification of NBD-GlcCer (**C**), NBD-Cer (**D**), and NBD-hexanoic acid (**E**), n≥4, ± SEM. Variability was increased in the NBD-Cer analyses due to close migration near the solvent front, thereby inconsistently elevating the

background. A repeated measures 2-way ANOVA was used to assess variance between genotypes, and comparisons were made with Tukey's post hoc test. No significant differences in NBD-lipid metabolism were found between the genotypes ($p>0.05$). Representative images were selected to most clearly illustrate the consistent lack of NBD-GlcCer metabolism. (**F**) Total fluorescent signal was assessed in each lane to examine the all NBD-lipid extracts per sample. Signal was collected from spot to ceramide front, as indicated by the dashed box in (**B**). Signal in the 0min lane was set at 1.0, and 30min and 120min lanes were normalized to this value and compared. Total fluorescent signal did not significantly change between samples, as tested by a one-way ANOVA with Tukey's comparison, $n\geq4$. These data suggest that equivalent amounts of NBD-lipid were extracted when sampling within each genotype.

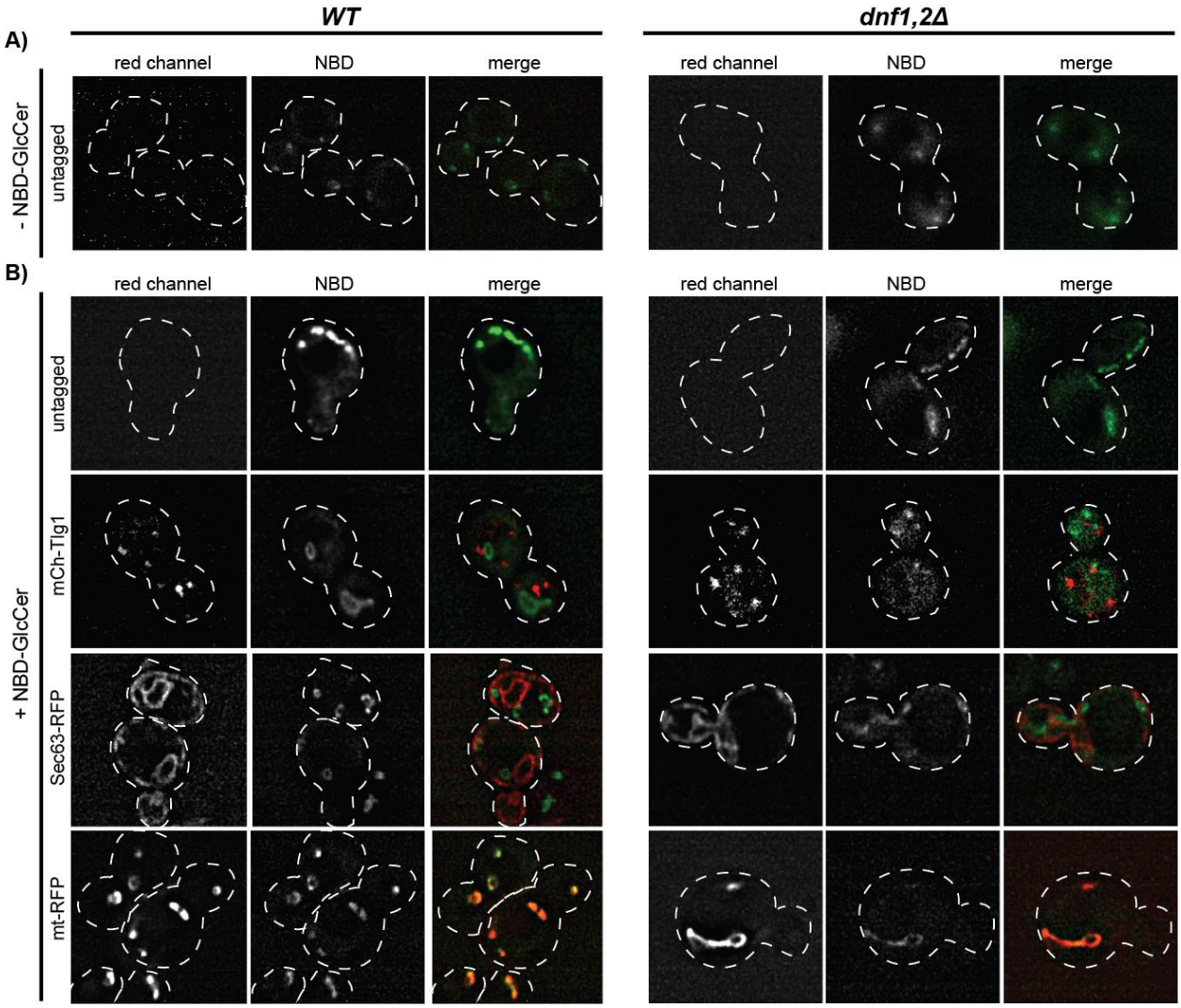

Figure S4. NBD-GlcCer localizes to the mitochondria. The NBD fluorophore photobleaches rapidly during microscopy, therefore images have been scaled to present localization rather than intensity. (A) *WT* (BY4171) and *dnf1,2*Δ cells were imaged without markers and lipids to define channel autofluorescence. (B) NBD-GlcCer was added as detailed in the Materials and Methods, to each strain featuring red fluorescent markers for endosomes (mCh-Tlg1), ER (Sec63-RFP), and mitochondria (mt-RFP). Images are representative of 3 experiments.

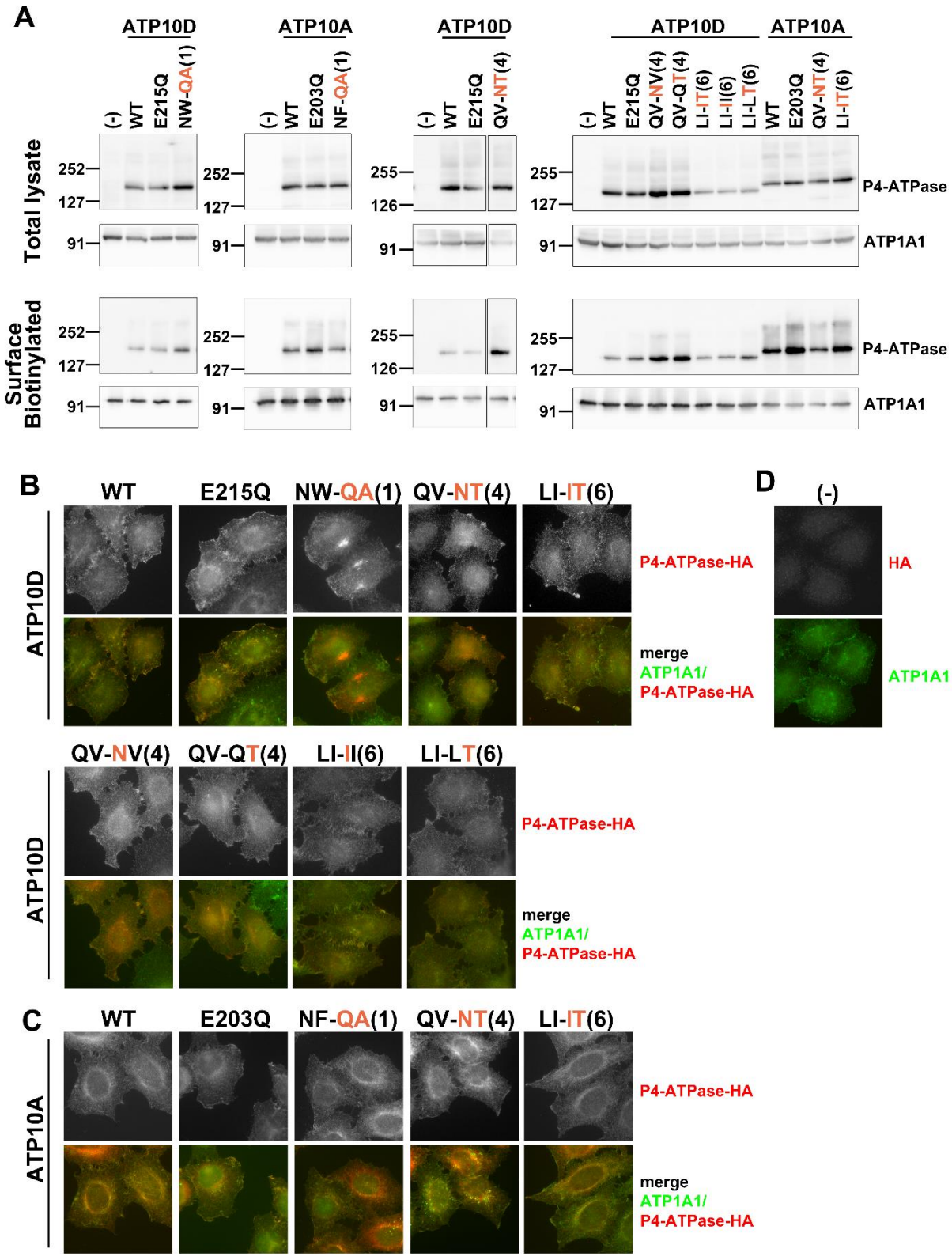
A
ATP10D
ATP10A
ATP10D
ATP10D
ATP10A
(-)
WT
E215Q
NW-QA(1)
E203Q
NF-QA(1)
QV-NT(4)
QV-NV(4)
QV-QT(4)
LI-IT(6)
LI-II(6)
LI-LT(6)
Total lysate
Surface Biotinylated
252
127
91
255
126
P4-ATPase
ATP1A1
B
WT
E215Q
NW-QA(1)
QV-NT(4)
LI-IT(6)
ATP10D
P4-ATPase-HA
merge
ATP1A1/
P4-ATPase-HA
QV-NV(4)
QV-QT(4)
LI-II(6)
LI-LT(6)
C
E203Q
ATP10A
D
HA
ATP1A1

Figure S5. ATP10A and ATP10D constructs localized to the PM in HeLa cells. HeLa cells stably expressing C-terminally HA-tagged ATP10A, ATP10D, and each mutant (indicated) were analyzed. The NBD-lipid transport profiles of each of these constructs were tested in Figs. 2 and 6, and these data evaluate their respective protein levels and localization. The mutations assessed included ATPase mutants ($ATP10A^{E203Q}$, $ATP10D^{E15Q}$), TM1 mutations ($ATP10A^{NF\text{-}QA}$, $ATP10D^{NW\text{-}QA}$), TM4 mutations ($ATP10A^{QV\text{-}NT}$, $ATP10D^{QV\text{-}NT}$, $ATP10D^{QV\text{-}NV}$, $ATP10D^{QV\text{-}QT}$), and TM6 mutations ($ATP10A^{LI\text{-}LT}$, $ATP10D^{LI\text{-}IT}$, $ATP10D^{LI\text{-}II}$, and $ATP10D^{LI\text{-}LT}$). TM is numbered in parenthesis. (-) indicates parental HeLa cells. (**A**) The total expression level of the P4-ATPase in each cell was analyzed by immunoblotting with anti-HA and anti-ATP1A1 antibodies (as an internal control). 10 % of the input of the biotinylation reaction was loaded in each lane. The cell surface level of the P4-ATPase in each cell was analyzed after surface biotinylation. Data shown here are representative of at least two independent experiments. (**B**-**D**) Cells were fixed, permeabilized, and incubated with anti-HA and anti-ATP1A1 antibodies followed by Cy3-conjugated anti-rat and Alexa Fluor 488-conjugated anti-rabbit secondary antibodies. ATP1A1 used as a marker for the plasma membrane.

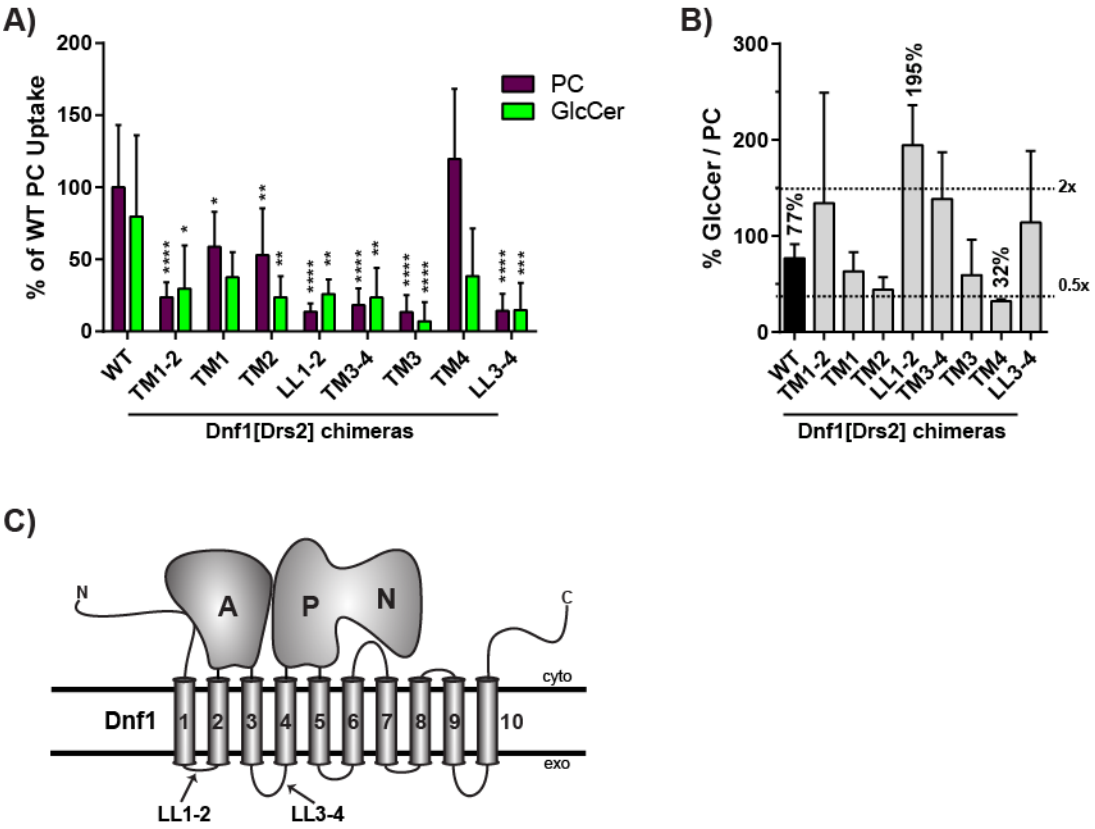

Figure S6. Dnf1[Drs2] chimeras demonstrate that the lumenal regions of Dnf1 TM1-2 and TM4 help select NBD-GlcCer. TM and loop regions of Dnf1 were replaced with Drs2 coding sequence as previously described (4) and examined for NBD-PC and NBD-GlcCer uptake (**A**) and preference (**B**). (**A**) Many of the chimeras exhibited a general decrease in substrate uptake, yet two chimeras shifted the % GlcCer/PC substrate preference two-fold: Dnf1[LL1-2] and Dnf1[TM4] (**B**). A cartoon of Dnf1 is presented in (**C**) to illustrate the regions of the enzyme modified by the chimera approach, with the defining P-Type ATPase cytosolic "A," "P," and "N" domains annotated. Variance was assessed among data sets using One-way ANOVAs, and comparisons to WT made with Tukey's post hoc analysis. $n \geq 8 \pm$ SD, * indicates $p<0.05$, **$p<0.01$, ***$p<0.001$, ****$p<0.0001$.

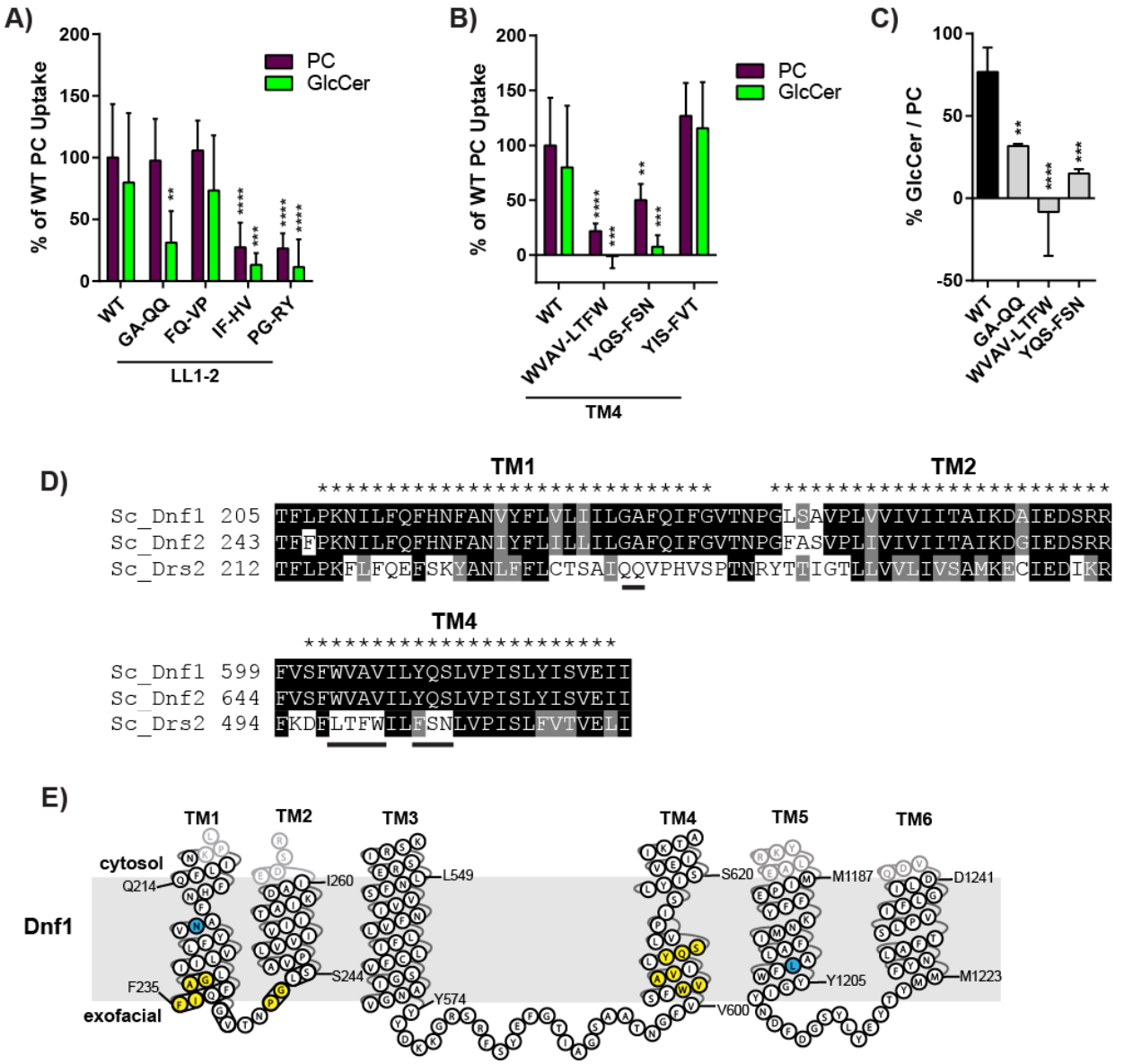

Figure S7. Dnf1 substitutions establish the involvement of an exofacial GA and YQS motif in GlcCer selection. Targeted examinations of the Dnf1[LL1-2] (**A**) and Dnf1[TM4] (**B**) regions revealed that Dnf1[GA-QQ], Dnf1[WVAV-LTFW] and Dnf1[YQS-FSN] significantly decreased GlcCer preference (**C**) (n≥9, ± SD). An alignment of TM 1, 2 and 4 from *S. cerevisiae* Dnf1, Dnf2, and Drs2 with TM domains indicated with asterisks and key substrate selective sequences underlined (**D**). Shown is a topology diagram of Dnf1 TM segments 1-6 with residues that enhance GlcCer transport highlighted in Blue and residues that inhibit GlcCer transport highlighted in Green (B). Variance was assessed among data sets using One-way ANOVAs, and comparisons to WT made with Tukey's post hoc analysis. * indicates $p<0.05$, ** $p<0.01$, *** $p<0.001$, **** $p<0.0001$.

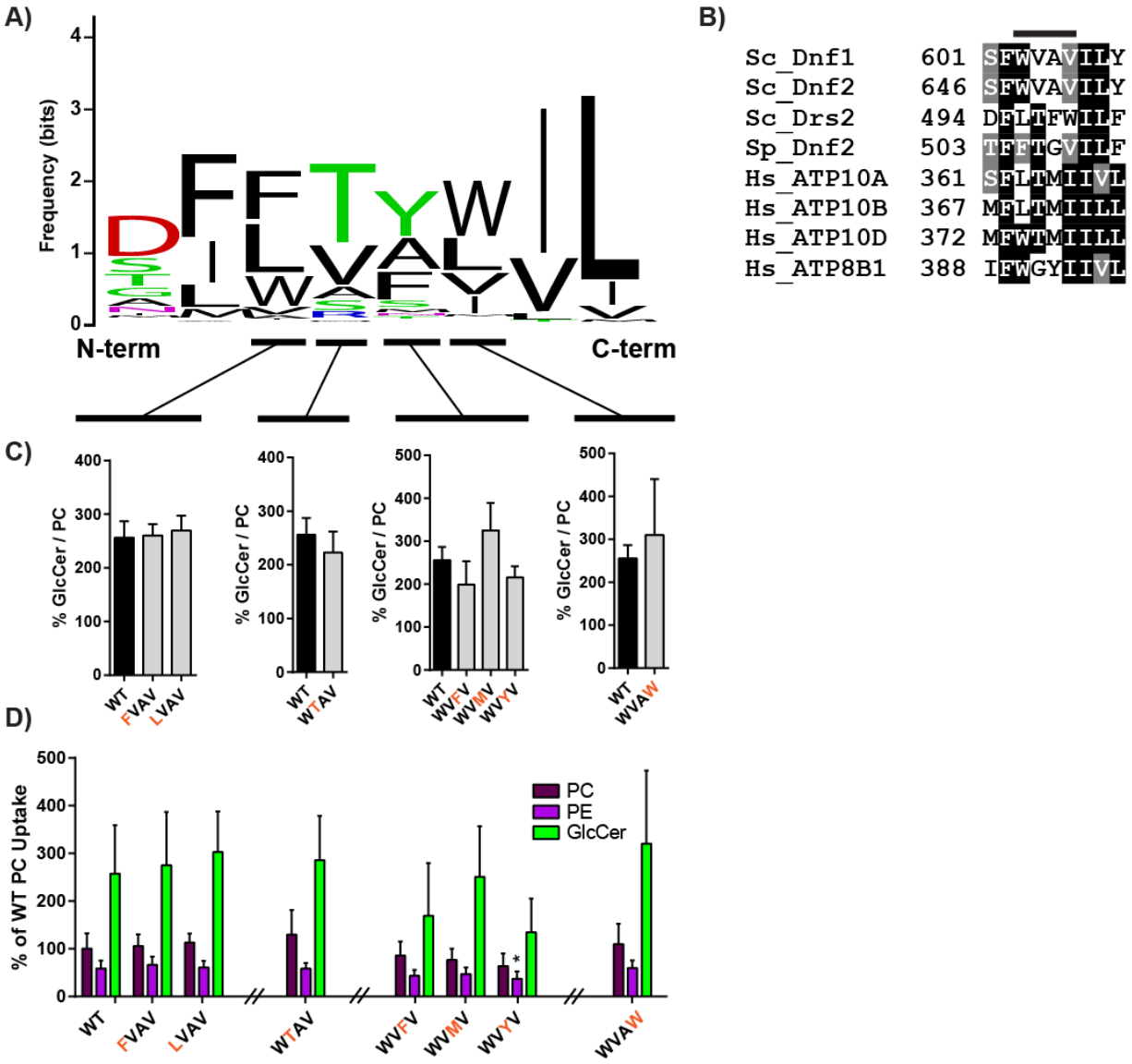

Figure S8. Single substitutions in the exofacial stretch of Dnf2 TM4 do not influence GlcCer transport. (**A**) A sequence logo was created from an alignment of TM4 of P4-ATPases from different organisms, with letter size representing residue frequency and color denoting chemical characteristics. (**A**) Hydrophilic residues are **green** and **purple**, acidic residues in **red**, and hydrophobic residues are indicated in **black**. (**B**) A focused alignment comparing a region of TM4 from *S.cerevisiae*, *H.sapiens*, and *S.pombe*, highlighting the **WVAV** motif that was previously altered in *S.c. Dnf1* (fig. S7). Dissecting the four positions of the **WVAV** motif reveals that single substitutions at various positions along this stretch do not significantly alter GlcCer preference (**C**) or recognition (**D**). (**D**) Substitutions in this region do not appear to alter glycerophospholipid recognition either, beyond a third position Ala-to-Tyr substitution at WV**A**V that reduces PE recognition. Variance was assessed among data sets using One-way ANOVAs, and comparisons to WT made with Tukey's post hoc analysis. Although the WVAV positions in (**C**) are presented in separate panels, their statistical variance was tested together. $n \geq 9$, ± SD, * indicates $p<0.05$.

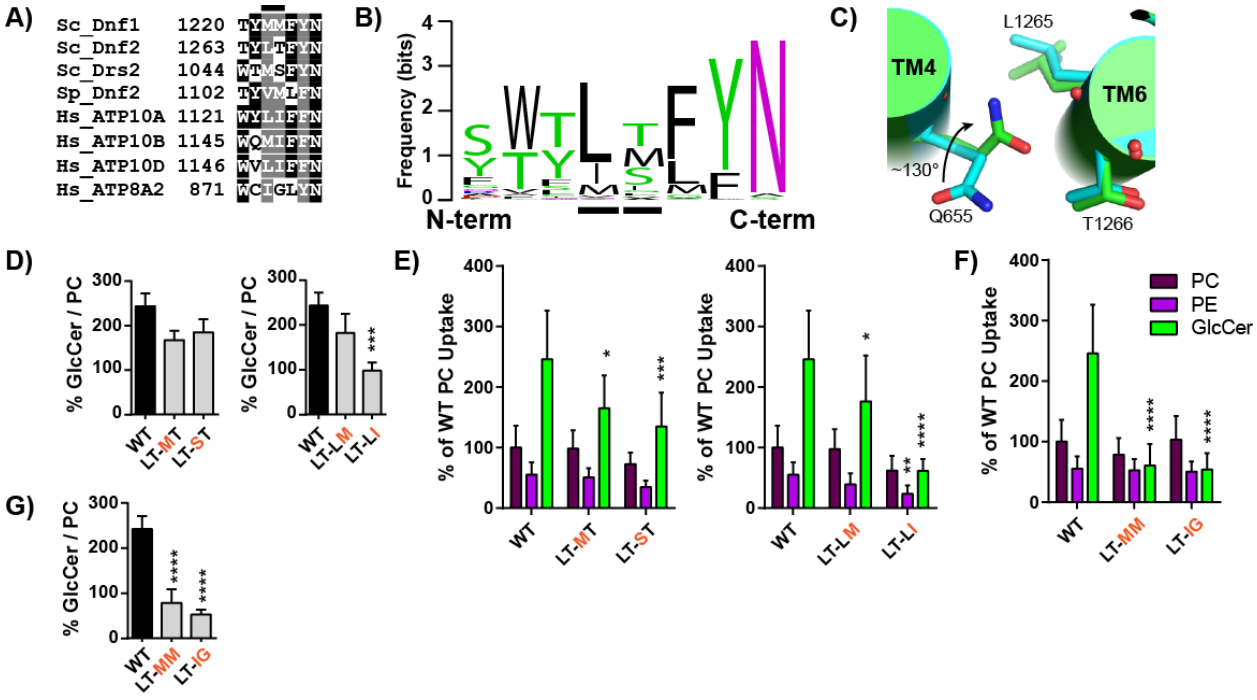

Figure S9. The TM6 LT motif specifically modulates GlcCer transport. A focused alignment comparing a region of TM6 from *S.cerevisiae*, *H.sapiens*, and *S.pombe*, highlighting the **LT** motif (**A**). A sequence logo was created from an alignment of TM6 of P4-ATPases from different organisms, with letter size representing residue frequency and color denoting chemical differences (**B**). Hydrophilic residues are **green** and **purple**, acidic residues in **red**, and hydrophobic residues are indicated in **black** (**B).** Homology model of Dnf2 with Q655 indicated in sticks and colored by element (**C**). The original predicted positioning of Q655 was sculpted as described in the methods, to rotate the residue around the β-γ carbon. The original position and associated structures are colored cyan, and the repositioned model shown in green (**C**). Dissecting the first and second positions of the LT motif reveals that substitutions in the second position can reduce GlcCer preference (**D**), while both positions alter GlcCer recognition (**E**). Double-substitutions were created to examine *S.c. Dnf1* and *H. sapiens ATP8A1/2* sequences in the context of the *S. cerevisiae Dnf2*, and it was found that these compound mutations reduced GlcCer selection (**F**) and preference (**G**) without altering the known glycerophospholipid substrates (**F**). Variance was assessed among data sets using One-way ANOVAs, and comparisons to WT made with Tukey's post hoc analysis. Although first and second position LT analyses are presented in different panels (**D**, **E**), their statistical variance was tested together. * indicates $p<0.05$, ** $p<0.01$, *** $p<0.001$, **** $p<0.0001$.

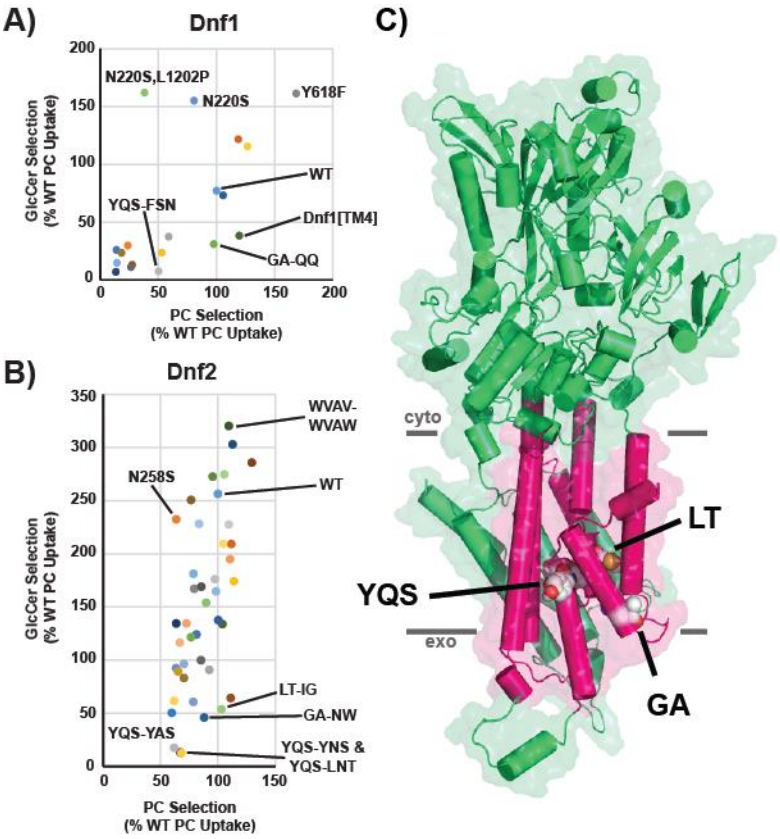

Figure S10. GlcCer-determining residues on TM1, TM4, and TM6 cluster on Dnf1 homology model. Scatter plots present the mean PC (x-axis) and GlcCer (y-axis) selection by various chimera and point mutation constructs created from *S.c.* Dnf1 (**A**) and *S.c.* Dnf2 (**B**). Enzyme mutants of interest are called out in the scatter plot, and a full table of all mutations are presented in the supplement (Table S3 and S4). (**C**) Homology model of Dnf1 (from PDB: 3W5D) with TM 1–6 shown as pink cylinders, the rest of the protein colored green, surface shown, and three key primary structural motifs; TM1-GA, TM4-YQS, and TM6-LT; represented in spheres and colored by element; PM boundaries are indicated. Note the predicted 3D clustering of GA, YQS, and LT motifs near the mid-to-exofacial aspect of the TM domain.

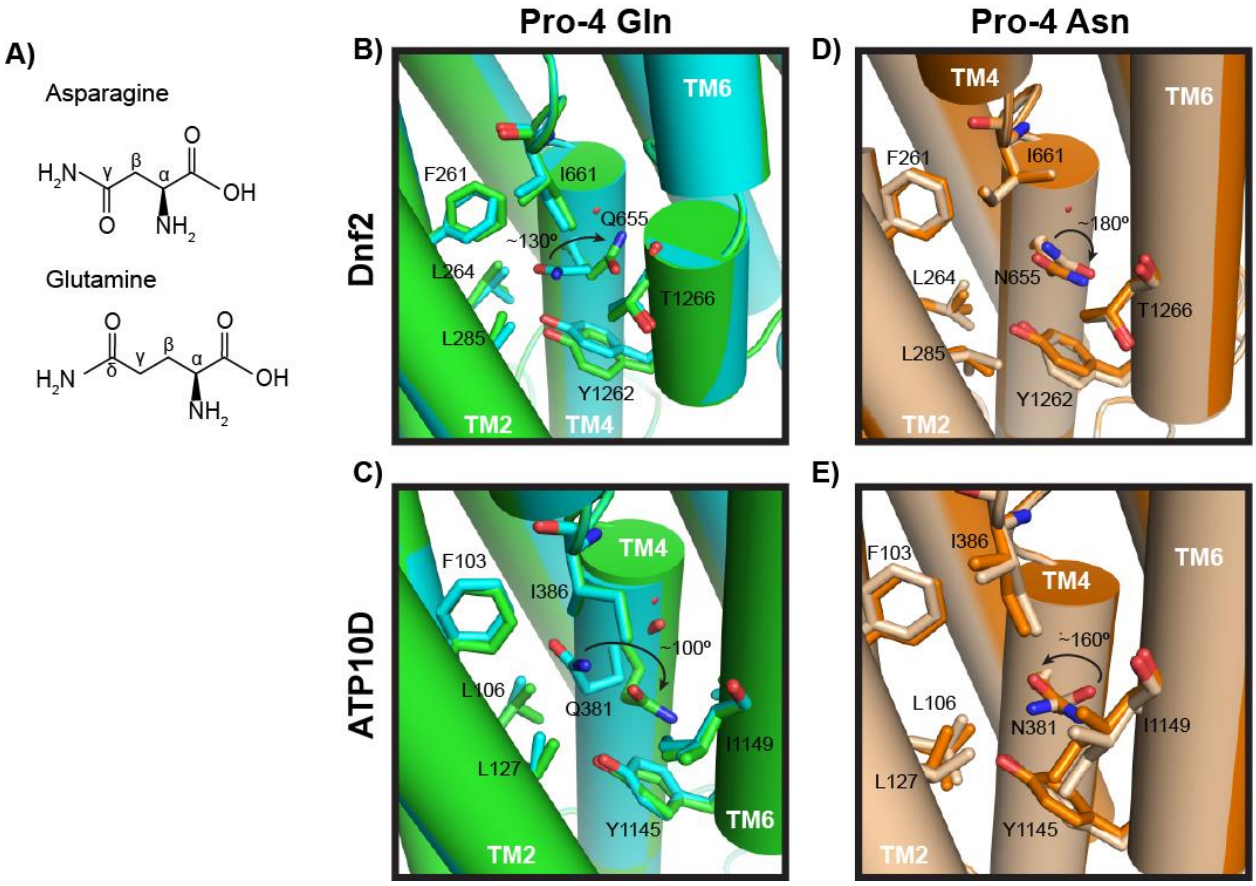

Figure S11. Pro-4 glutamine is predicted to be rotationally flexible within Dnf2 and ATP10D. A chemical comparison of the amino acids asparagine and glutamine with labeled carbons for reference (**A**). Homology models were generated of Dnf2 and ATP10D, and the Pro-4 residue is depicted in (**B**) and (**C**), respectively. The Pro-4 glutamine was rotated around the β-γ carbon bond as described in the methods, with the original model positions colored cyan and the repositioned model colored green. Important residues impacted by Pro-4 movements are shown in sticks and colored by element. Similarly, homology models of Pro-4 asparagine mutants of Dnf2 and ATP10D were generated, and depicted in (**D**) and (**E**), respectively. The Pro-4 asparagine was rotated around the the β-γ carbon bond, with the original position colored orange, and the rotated position colored wheat. All model images are oriented with cytofacial aspect of the TM domain up and the exofacial aspect down.

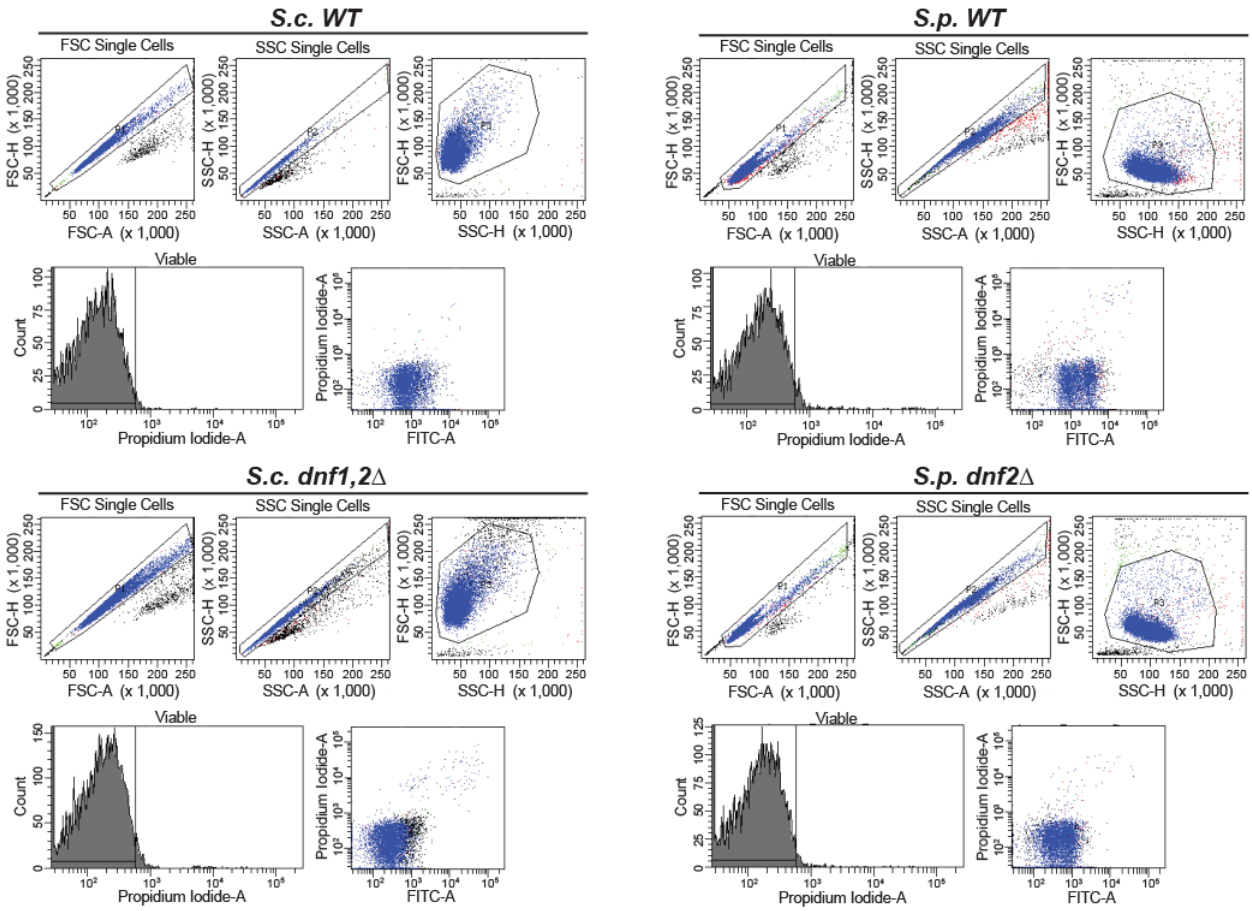

Figure S12. Gate settings used for comparative *S.cerevisiae* and *S.pombe* flow cytometry analysis. Flow cytometry gates were set specifically to facilitate intra-experimental comparisons of different fungal species. Presented are the raw data and gate settings from a single experiment performed, comparing NBD-GlcCer uptake in *S.cerevisiae WT* and *dnf1,2Δ*, and *S.pombe WT* and *dnf2Δ*. Three initial forward and side scatter gates were used to isolate single cell populations, PI staining used to select viable cells, and FITC signal was examined. Note the gross shift in FITC signal between the WT and respective P4-ATPase mutants.

Table S1. Yeast and human cell strains used in this study.

Strain	Genotype	Plasmid	Source
S. cerevisiae			
BY4741	MATa his3Δ1 leu2Δ0 ura3Δ0 met15Δ0	none	ATCC
BY4741 YER166W	MATa his3Δ1 leu2Δ0 ura3Δ0 met15Δ0 dnf1Δ	none	ATCC
BY4741 YDR093W	MATa his3Δ1 leu2Δ0 ura3Δ0 met15Δ0 dnf2Δ	none	ATCC
PFY3275F	MATa his3Δ1 leu2Δ0 ura3Δ0 met15Δ0 dnf1Δ dnf2Δ	none	(5)
BRY1521 A	PFY3275F	pRS313	This Study
BRY1522 A	PFY3275F	pRS313-Dnf1	This Study
BRY1523 A	PFY3275F	pRS313-Dnf2	This Study
BRY1104.0 G	PFY3275F	pRS313	(6)
BRY1104.1 G	PFY3275F	pRS313-Dnf1	(6)
BRY1104.8 G	PFY3275F	pRS313-Dnf1 N220S	(6)
BRY1104.8 D	PFY3275F	pRS313-Dnf1 N220S,L1202P	(6)
RBY640	PFY3275F	pRS313-Dnf1[TM1-2]	(4)
RBY6206	PFY3275F	pRS313-Dnf1[TM1]	(7)
RBY6209	PFY3275F	pRS313-Dnf1[TM2]	(7)
RBY637	PFY3275F	pRS313-Dnf1[LL1-2]	(7)
RBY667	PFY3275F	pRS313-Dnf1[TM3-4]	(4)
RBY676	PFY3275F	pRS313-Dnf1[TM3]	(4)
RBY673	PFY3275F	pRS313-Dnf1[TM4]	(4)
RBY679	PFY3275F	pRS313-Dnf1[LL3-4]	(4)
RBY607	PFY3275F	pRS313-Dnf1 GA-QQ	(7)
RBY610	PFY3275F	pRS313-Dnf1 FQ-VP	(7)
RBY616	PFY3275F	pRS313-Dnf1 IF-HV	(7)
RBY625	PFY3275F	pRS313-Dnf1 PG-RY	(7)
RBY682	PFY3275F	pRS313-Dnf1 WVAV-LTFW	(4)
RBY685	PFY3275F	pRS313-Dnf1 YQS-FSN	(4)
RBY688	PFY3275F	pRS313-Dnf1 YIS-FVT	(4)
BRY2104 A	PFY3275F	pRS313-Dnf2 GA-QQ	This Study
BRY2108 A	PFY3275F	pRS313-Dnf2 GA-NA	This Study
BRY2106 A	PFY3275F	pRS313-Dnf2 GA-QA	This Study
BRY2107 A	PFY3275F	pRS313-Dnf2 GA-GW	This Study
BRY2105 A	PFY3275F	pRS313-Dnf2 GA-NW	This Study
BRY2109 A	PFY3275F	pRS313-Dnf2 GA-QS	This Study
BRY2220 A	PFY3275F	pRS313-Dnf2 WVAV-FVAV	This Study
BRY2221 A	PFY3275F	pRS313-Dnf2 WVAV-LVAV	This Study

BRY2222 A	PFY3275F	pRS313-Dnf2 WVAV-WTAV	This Study
BRY2223 A	PFY3275F	pRS313-Dnf2 WVAV-WVFV	This Study
BRY2224 A	PFY3275F	pRS313-Dnf2 WVAV-WVMV	This Study
BRY2225 A	PFY3275F	pRS313-Dnf2 WVAV-WVYV	This Study
BRY2226 A	PFY3275F	pRS313-Dnf2 WVAV-WVAW	This Study
BRY2127 A	PFY3275F	pRS313-Dnf2 YQS-FQS	This Study
BRY2122 A	PFY3275F	pRS313-Dnf2 YQS-LQS	This Study
BRY2128 A	PFY3275F	pRS313-Dnf2 YQS-YAS	This Study
BRY2123 A	PFY3275F	pRS313-Dnf2 YQS-YNS	This Study
BRY2124 A	PFY3275F	pRS313-Dnf2 YQS-YQN	This Study
BRY2125 A	PFY3275F	pRS313-Dnf2 YQS-YQT	This Study
BRY2126 A	PFY3275F	pRS313-Dnf2 YQS-YQV	This Study
BRY2110 A	PFY3275F	pRS313-Dnf2 YQS-FSN	This Study
BRY2111 A	PFY3275F	pRS313-Dnf2 YQS-LQV	This Study
BRY2112 A	PFY3275F	pRS313-Dnf2 YQS-FQN	This Study
BRY2113 A	PFY3275F	pRS313-Dnf2 YQS-LNT	This Study
BRY2202 A	PFY3275F	pRS313-Dnf2 F261S	This Study
BRY2203 A	PFY3275F	pRS313-Dnf2 L264Q	This Study
BRY2204 A	PFY3275F	pRS313-Dnf2 L264S	This Study
BRY2205 A	PFY3275F	pRS313-Dnf2 L285S	This Study
BRY2206 A	PFY3275F	pRS313-Dnf2 L605S	This Study
BRY2207 A	PFY3275F	pRS313-Dnf2 C609A	This Study
BRY2208 A	PFY3275F	pRS313-Dnf2 S1257Q	This Study
BRY2209 A	PFY3275F	pRS313-Dnf2 Y1262Q	This Study
BRY2210 A	PFY3275F	pRS313-Dnf2 Y1262S	This Study
BRY2234 A	PFY3275F	pRS313-Dnf2 T1266I	This Study
BRY2211 A	PFY3275F	pRS313-Dnf2 L1270S	This Study
BRY2231 A	PFY3275F	pRS313-Dnf2 LT-MT	This Study
BRY2232 A	PFY3275F	pRS313-Dnf2 LT-ST	This Study
BRY2233 A	PFY3275F	pRS313-Dnf2 LT-LM	This Study
BRY2235 A	PFY3275F	pRS313-Dnf2 LT-MM	This Study
BRY2236 A	PFY3275F	pRS313-Dnf2 LT-IG	This Study
BRY2103 A	PFY3275F	pRS313-Dnf2 N220S	This Study
BRY3001 A	BY4741	pSM1959-Sec63-RFP	This Study
BRY3002 A	PFY3275F	pSM1959-Sec63-RFP	This Study
BRY3003 A	BY4741	pRS313-Tlg1-mCherry	This Study
BRY3004 A	PFY3275F	pRS313-Tlg1-mCherry	This Study
BRY3005 A	BY4741	pRS305-mt-RFP	This Study
BRY3006 A	PFY3275F	pRS305-mt-RFP	This Study
SCY119	MATα his3Δ1 leu2Δ0 ura3Δ0 met15Δ0 lem3Δ	None	(4)
RBY9701	PFY3275F lem3Δ	None	(4)

S.pombe			
KGY246	ade6-m210 leu1-32 ura4-D18 h-	none	Gould Lab
S.p. dnf2Δ	SPAC 24B11.12C*::kanMX4 h+ ade6-M210 ura4-D18 leu1–32*	none	Gould Lab
H.sapiens			
HeLa			
HeLa/ATP8A1-HA		pMx/neo-hATP8A1-HA	This Study
HeLa/ATP8B1-HA		pMx/neo-hATP8B1-HA	(2)
HeLa/ATP8B2-HA		pMx/neo-hATP8B2-HA	(2)
HeLa/ATP8B4-HA		pMx/neo-hATP8B4-HA	This Study
HeLa/ATP10A-HA		pMx/neo-hATP10A-HA	(8)
HeLa/ATP10D-HA		pMx/neo-hATP10D-HA	(8)
HeLa/ATP11A-HA		pMx/neo-hATP11A-HA	(2)
HeLa/ATP11C-HA		pMx/neo-hATP11C-HA	(2)
HeLa/ATP10A(E203Q)-HA		pMx/neo-hATP10A(E203Q)-HA	(8)
HeLa/ATP10D(E215Q)-HA		pMx/neo-hATP10D(E215Q)-HA	This Study
HeLa/ATP10D(NW-QA)-HA		pMx/neo-hATP10D(NW-QA)-HA	This Study
HeLa/ATP10D(QV-NT)-HA		pMx/neo-hATP10D(QV-NT)-HA	This Study
HeLa/ATP10D(Q381N)-HA		pMx/neo-hATP10D(Q381N)-HA	This Study
HeLa/ATP10D(V382T)-HA		pMx/neo-hATP10D(V382T)-HA	This Study
HeLa/ATP10D(LI-IT)-HA		pMx/neo-hATP10D(LI-IT)-HA	This Study
HeLa/ATP10D(L1148I)-HA		pMx/neo-hATP10D(L1148I)-HA	This Study
HeLa/ATP10D(I1149T)-HA		pMx/neo-hATP10D(I1149T)-HA	This Study
HeLa/ATP10A(NF-QA)-HA		pMx/neo-hATP10A(NF-QA)-HA	This Study
HeLa/ATP10A(QV-NT)-HA		pMx/neo-hATP10A(QV-NT)-HA	This Study
HeLa/ATP10A(LI-IT)-HA		pMx/neo-hATP10A(LI-IT)-HA	This Study

Table S2. Plasmids used in this study.

Plasmid	**Notes**	**Source**
pRS313		(9)
pRS313-Dnf1		(10)

pRS313-Dnf1 N220S		(6)
pRS313-Dnf1 N220S,L1202P		(6)
pRS313-Dnf1[TM1-2]	Chimera enzyme with [Drs2]	(4)
pRS313-Dnf1[TM1]	Chimera enzyme with [Drs2]	(7)
pRS313-Dnf1[TM2]	Chimera enzyme with [Drs2]	(7)
pRS313-Dnf1[LL1-2]	Chimera enzyme with [Drs2]	(7)
pRS313-Dnf1[TM3-4]	Chimera enzyme with [Drs2]	(4)
pRS313-Dnf1[TM3]	Chimera enzyme with [Drs2]	(7)
pRS313-Dnf1[TM4]	Chimera enzyme with [Drs2]	(7)
pRS313-Dnf1[LL3-4]	Chimera enzyme with [Drs2]	(4)
pRS313-Dnf1 GA-QQ	G230Q,A231Q	(7)
pRS313-Dnf1 FQ-VP	F232V,Q233P	(7)
pRS313-Dnf1 IF-HV	I234H,F235V	(7)
pRS313-Dnf1 PG-RY	P240R,G241Y	(7)
pRS313-Dnf1 WVAV-LTFW	W603L,V604T,A605F,V606W	(4)
pRS313-Dnf1 YQS-FSN	Y609F,Q610S,S611N	(4)
pRS313-Dnf1 YIS-FVT	Y618F,I619V,S620T	(4)
pRS313-Dnf2 GA-QQ	G268Q,A269Q	This study
pRS313-Dnf2 GA-NA	G268N	This study
pRS313-Dnf2 GA-QA	G268Q	This study
pRS313-Dnf2 GA-GW	A269W	This study
pRS313-Dnf2 GA-NW	G268N,A269W	This study
pRS313-Dnf2 GA-QS	G268Q,A269S	This study
pRS313-Dnf2 WVAV-FVAV	W648F	This study
pRS313-Dnf2 WVAV-LVAV	W648L	This study
pRS313-Dnf2 WVAV-WTAV	V649T	This study
pRS313-Dnf2 WVAV-WVFV	A650F	This study
pRS313-Dnf2 WVAV-WVMV	A650M	This study
pRS313-Dnf2 WVAV-WVYV	A650Y	This study
pRS313-Dnf2 WVAV-WVAW	V651W	This study
pRS313-Dnf2 YQS-FQS	Y654F	This study
pRS313-Dnf2 YQS-LQS	Y654L	This study
pRS313-Dnf2 YQS-YAS	Q655A	This study
pRS313-Dnf2 YQS-YNS	Q655N	This study
pRS313-Dnf2 YQS-YQN	S656N	This study
pRS313-Dnf2 YQS-YQT	S656T	This study
pRS313-Dnf2 YQS-YQV	S656V	This study
pRS313-Dnf2 YQS-FSN	Y654F,Q655S,S656N	This study
pRS313-Dnf2 YQS-LQV	Y654L,S656V	This study
pRS313-Dnf2 YQS-FQN	Y654F,S656N	This study
pRS313-Dnf2 YQS-LNT	Y654L,Q655N,S654T	This study
pRS313-Dnf2 F261S		This study
pRS313-Dnf2 L264Q		This study
pRS313-Dnf2 L264S		This study
pRS313-Dnf2 L285S		This study
pRS313-Dnf2 L605S		This study
pRS313-Dnf2 C609A		This study
pRS313-Dnf2 S1257Q		This study
pRS313-Dnf2 Y1262Q		This study

pRS313-Dnf2 Y1262S		This study
pRS313-Dnf2 T1266I	i.e. LT-LI mutant	This study
pRS313-Dnf2 L1270S		This study
pRS313-Dnf2 LT-MT	L1265M	This study
pRS313-Dnf2 LT-ST	L1265S	This study
pRS313-Dnf2 LT-LM	T1266M	This study
pRS313-Dnf2 LT-MM	L1265M, T1266M	This study
pRS313-Dnf2 LT-IG	L1265I, T1266G	This study
pRS313-Dnf2 N258S	Homologous to Dnf1[N220S]	This study
pSM1959-Sec63-RFP	Red ER marker	(11)
pRS313-Tlg1-mCherry	Red trans-golgi marker	(12)
pRS305-mt-RFP	Red mitochondrial marker	(13)
pMx/neo-hATP8A1-HA		(2)
pMx/neo-hATP8B1-HA		(2)
pMx/neo-hATP8B2-HA		(2)
pMx/neo-hATP8B4-HA		This Study
pMx/neo-hATP9A-HA		This Study
pMx/neo-hATP9B-HA		This Study
pMx/neo-hATP10A-HA		(8)
pMx/neo-hATP10B-HA		This Study
pMx/neo-hATP10D-HA		(8)
pMx/neo-hATP11A-HA		(2)
pMx/neo-hATP11B-HA		This Study
pMx/neo-hATP11C-HA		(2)
pMx/neo-hATP10A(E203Q)-HA	E203Q	(8)
pMx/neo-hATP10D(E215Q)-HA	E215Q	This Study
pMx/neo-hATP10D(NW-QA)-HA	N110Q, W111A	This Study
pMx/neo-hATP10D(QV-NT)-HA	Q381N, V382T	This Study
pMx/neo-hATP10D(Q381N)-HA	Q381N, i.e. QV-NV mutant	This Study
pMx/neo-hATP10D(V382T)-HA	V382T, i.e. QV-QT mutant	This Study
pMx/neo-hATP10D(LI-IT)-HA	L1148I, I1149T	This Study
pMx/neo-hATP10D(L1148I)-HA	L1148I, i.e. LI-II mutant	This Study
pMx/neo-hATP10D(I1149T)-HA	I1149T, i.e. LI-LT mutant	This Study
pMx/neo-hATP10A(NF-QA)-HA	N98Q, F99A	This Study
pMx/neo-hATP10A(QV-NT)-HA	Q370N, V371T	This Study
pMx/neo-hATP10A(LI-IT)-HA	L1123I, I1124T	This Study

Table S3. Concatenated mean PC and GlcCer selection for all Dnf1 mutants.

Dnf1 Variant	PC Selection (% WT PC)	GlcCer Selection (% WT PC)
Dnf1 WT	100	77.24
Dnf1[TM1-2]	23.67	29.83
Dnf1[TM1]	58.79	37.55
Dnf1[TM2]	52.86	23.67
Dnf1[LL1-2]	13.83	25.99
Dnf1[GA-QQ]	97.53	31.01
Dnf1[FQ-VP]	105.7	73.28
Dnf1[IF-HV]	27.36	13.11
Dnf1[PG-RY]	26.36	11.29
Dnf1[TM3-4]	18.22	23.55
Dnf1[TM3]	13.39	7.055
Dnf1[TM4]	119.6	38.39
Dnf1[LL3-4]	14.29	14.8
Dnf1[WVAV-LTFW]	21.93	-0.8532
Dnf1[YQS-FSN]	50.04	7.551
Dnf1[YIS-FVT]	126.7	115.6
Dnf1 N220S	80.67	155.2
Dnf1 N220S,L1202P	38	162.1
Dnf1[GA-QQ]	118.4	34
Dnf1 N550S	118.8	121.8
Dnf1 Y618F	168.5	161.4

Table S4. Concatenated mean PC and GlcCer selection for all Dnf2 mutants.

Dnf2 Variant	PC Selection (% WT PC)	GlcCer Selection (% WT PC)
Dnf2 WT	100	256.3
Dnf2 N220S	63.62	232.3
Dnf2 GA-QA	92.51	90.68
Dnf2 GA-GW	113.9	174.1
Dnf2 GA-NA	81.27	124
Dnf2 GA-QQ	76.5	121.5
Dnf2 GA-NW	88.04	45.88
Dnf2 YQS-FSN	111.1	64.24
Dnf2 YQS-LQV	85.28	99.8
Dnf2 YQS-FQN	70.28	83.11
Dnf2 YQS-LNT	67.32	12.91
Dnf2 GA-QS	103.9	133.8
Dnf2 YQS-FQS	78.62	181.2
Dnf2 YQS-LQS	110.5	194.8
Dnf2 YQS-YAS	61.8	17.44
Dnf2 YQS-YNS	68.21	12.33
Dnf2 YQS-YQN	63.57	92.39
Dnf2 YQS-YQT	89.8	153.8
Dnf2 YQS-YQV	59.83	50.32
Dnf2 F261S	111.6	209.2

Dnf2 L264Q	79.42	167.1
Dnf2 L264S	65.35	89.12
Dnf2 L285S	100.2	137.6
Dnf2 C609A	95.4	272.6
Dnf2 L605S	83.54	228.1
Dnf2 S1257Q	66.74	116.3
Dnf2 Y1262Q	109.4	227.5
Dnf2 Y1262S	104.6	209.3
Dnf2 L1270S	70.3	96.32
Dnf2 WVAV-FVAV	105.6	274.7
Dnf2 WVAV-LVAV	112.8	302.9
Dnf2 WVAV-WTAV	129.5	285.8
Dnf2 WVAV-WVFV	85.52	169
Dnf2 WVAV-WVMV	76.59	250.5
Dnf2 WVAV-WVYV	63.64	134.4
Dnf2 WVAV-WVAW	109.5	320.2
Dnf2 LT-MT	98.33	164.7
Dnf2 LT-ST	72.63	134.4
Dnf2 LT-LM	97.35	176
Dnf2 LT-LI	61.85	61.59
Dnf2 LT-MM	78.55	60.61
Dnf2 LT-IG	103	53.68

Supplemental References

1. Cromey DW (2010) Avoiding twisted pixels: ethical guidelines for the appropriate use and manipulation of scientific digital images. *Sci Eng Ethics* 16(4):639-667.
2. Takatsu H*, et al.* (2014) Phospholipid flippase activities and substrate specificities of human type IV P-type ATPases localized to the plasma membrane. *J Biol Chem* 289(48):33543-33556.
3. Crooks GE, Hon G, Chandonia JM, & Brenner SE (2004) WebLogo: a sequence logo generator. *Genome Res* 14(6):1188-1190.
4. Baldridge RD & Graham TR (2012) Identification of residues defining phospholipid flippase substrate specificity of type IV P-type ATPases. *Proc Natl Acad Sci U S A* 109(6):E290-298.
5. Hua Z & Graham TR (2003) Requirement for neo1p in retrograde transport from the Golgi complex to the endoplasmic reticulum. *Mol Biol Cell* 14(12):4971-4983.
6. Roland BP & Graham TR (2016) Directed evolution of a sphingomyelin flippase reveals mechanism of substrate backbone discrimination by a P4-ATPase. *Proc Natl Acad Sci U S A* 113(31):E4460-4466.
7. Baldridge RD & Graham TR (2013) Two-gate mechanism for phospholipid selection and transport by type IV P-type ATPases. *Proc Natl Acad Sci U S A* 110(5):E358-367.
8. Naito T*, et al.* (2015) Phospholipid Flippase ATP10A Translocates Phosphatidylcholine and Is Involved in Plasma Membrane Dynamics. *J Biol Chem* 290(24):15004-15017.
9. Sikorski RS & Hieter P (1989) A system of shuttle vectors and yeast host strains designed for efficient manipulation of DNA in Saccharomyces cerevisiae. *Genetics* 122(1):19-27.
10. Liu K, Hua Z, Nepute JA, & Graham TR (2007) Yeast P4-ATPases Drs2p and Dnf1p are essential cargos of the NPFXD/Sla1p endocytic pathway. *Mol Biol Cell* 18(2):487-500.

11. Metzger MB, Maurer MJ, Dancy BM, & Michaelis S (2008) Degradation of a cytosolic protein requires endoplasmic reticulum-associated degradation machinery. *J Biol Chem* 283(47):32302-32316.
12. Xu P, Baldridge RD, Chi RJ, Burd CG, & Graham TR (2013) Phosphatidylserine flipping enhances membrane curvature and negative charge required for vesicular transport. *J Cell Biol* 202(6):875-886.
13. Bhar D, Karren MA, Babst M, & Shaw JM (2006) Dimeric Dnm1-G385D interacts with Mdv1 on mitochondria and can be stimulated to assemble into fission complexes containing Mdv1 and Fis1. *J Biol Chem* 281(25):17312-17320.